

Influence of the Area of the Reflux Hole on the Performance of a Self-Priming Pump

Jiegang Mou¹, Fengye Zhang^{1,*}, Haoshuai Wang¹ and Denghao Wu¹

Abstract: The self-priming process of a pump involves a complex gas-liquid two-phase flow. Studying the distribution of gas and water and the evolution of their flow in the pump is of great importance to optimize this process and shorten the pump self-priming time. In the present study, a standard $k-\varepsilon$ turbulence model and a multiphase flow model have been used to simulate the self-priming pump process considering four different reflux hole areas. A comparison of the distribution of air and water distribution on the axial surface and inside the volume have been carried out for the different considered cases. The pattern formed by the streamlines at different times during the whole self-priming process has also been investigated. The results show that the velocity at the trailing edge of the impeller outlet is the largest. The flow in the pump cavity is complicated by the formation of vortices. The number, shape and location of the vortices change depending on the considered configuration.

Keywords: Self-priming pump, self-priming process, reflux hole, numerical simulation.

1 Introduction

As fluid machinery, self-priming pumps are widely used in the energy, power, petrochemical, national defense and municipal administration fields because of their optimal self-priming performance [Zhou and Zhang (2018); Fu (2018)]. They are especially suitable for flow irrigation, mobile work, frequent start-up work, difficult irrigation and so on [Mou, Wang, Wu et al. (2018); Kanute (2004); Yuan (2015); Yuan, Li and Shi (2011)]. The self-priming performance is one of the important indexes for evaluating a self-priming pump [Yuan, Li and Wang (2015); Li, Chen, Yuan et al. (2015); Jiang, Xie, Wang et al. (2014)]. The self-priming process includes a gas-liquid mixing process, a gas-liquid separation process and a recycling process of self-priming circulating liquid [Guan (2011); Xiao and Long (2015); Lu, Li and Zhan (2016)]. Many factors affect the complex process of a self-priming pump, such as the maximum circumferential velocity of the impeller, the size of the suction pipe, the area and position of the reflux hole, the gap between the outer edge of impeller and the tongue of the pump body, the volume of the liquid storage chamber and the volume of the gas-liquid separation chamber [Li, Jiang and Lu (2015); Pan, Zhang Li et al. (2014)]. Lin Rong et al.

¹ Department of Mechanical Engineering, Zhejiang University of Technology, Hangzhou, 310014, China.

* Corresponding Author: Fengye Zhang. Email: 15757172611@163.com.

[Lin, Yan and Xia (2014); Wang (2014)] summarized the factors that affect the self-priming performance of self-priming pumps and so provided a basis for the further study of self-priming pumps. An external mixing self-priming pump [Ma, Zhang, Cui et al. (2018), Huang, Su and Guo (2014); Wang, Shi, Li et al. (2016)] often uses a reflux hole to achieve the self-priming process, thus the reflux hole is very important in a self-priming pump. The location and geometric parameters of the reflux hole will affect the self-priming process. Whether the design of the reflux hole is reasonable or not will directly affect the self-priming performance. The leakage loss of the reflux hole equates to volume loss, so the efficiency of the self-priming pump will be affected.

Based on this, taking a 65zw30-40 self-priming pump as the research object, on the basis of keeping the position of the reflux hole unchanged, the gas-water distribution on the axial surface and the air volume fraction at the end of self-priming under different schemes were analyzed. Comparing the calculated results with the experimental data, the influence of the area of the reflux hole on the self-priming process is revealed. The influence of the area of the reflux hole on the performance is studied by analyzing the external characteristic curve, which provides a reference for the design and hydraulic optimization of self-priming pumps.

2 Modeling and numerical simulation

2.1 Modeling and meshing

The research object is a 65ZW30-40 self-priming pump. The main performance parameters are flow rate $Q=30$ m³/h, head $H=40$ m, speed $n=2900$ r/min and efficiency $\eta=55\%$; structural parameters: the number of blades is 2. The impeller inlet diameter $D_1=80$ mm, and the impeller outer diameter $D_2=185$ mm. The exit placement angle is $\beta_2=18^\circ$, and the specific speed is $n_s=60$. Tab. 1 presents the main parameter values of the impeller. Fig. 1 is a three-dimensional fluid domain model of each hydraulic component of the self-priming pump. It can be seen from the figure that the calculation domain of the self-priming pump mainly consists of the inlet section, the suction section, the front cover cavity, the impeller, the volute, the rear cover cavity, the pump body and the outlet section. To make the calculation result more consistent with the actual situation, the import section is lengthened and the inlet section is extended to 5 meters.

Table 1: Main parameters of the impeller

Specific speed (n_s)	Inlet diameter (D_1) mm	Outlet diameter (D_2) mm	Outlet width (b_2) mm	Exit placement angle (β_2)°
60	80	185	28	18

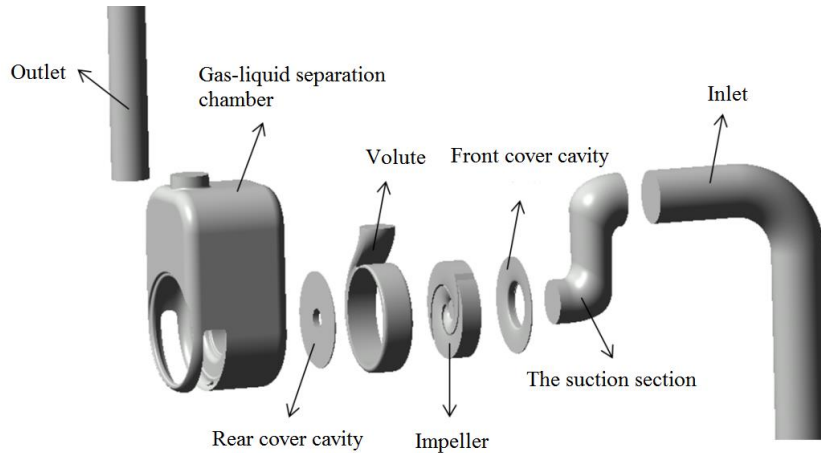


Figure 1: Calculation domain of the self-priming pump

Due to the complexity of the structure of a sewage self-priming pump, especially that the pump body, volute and impeller are composed of many complex curved surfaces, it is difficult to use a structural grid to mesh. After comprehensively considering the advantages and disadvantages of structural and non-structural grids and the complexity of the self-priming pump model, the ICEM software is used to decompose the calculation domain of the sewage self-priming pump. The meshing results are shown in Fig. 2.

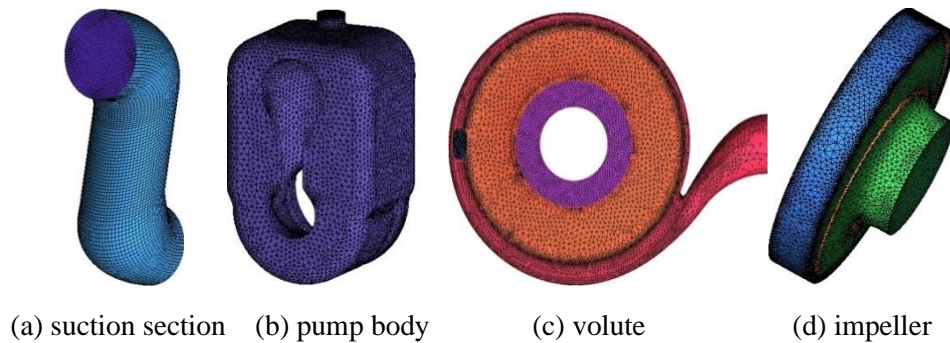


Figure 2: Calculation area of the sewage self-priming pump

2.2 Multiphase flow model and boundary conditions

In the self-priming process of the self-priming pump, air is regarded as a discrete phase. In addition to the water in the pump body, the inlet and outlet pipes are also filled with air. In the self-priming stage, the discrete phase is widely distributed, therefore, a mixture model is selected as the two-phase flow model [Wang, Wu, Si et al. (2009); Liu and Su (2017, 2009)].

(1) Continuity equation of mixtures:

$$\frac{\partial}{\partial t}(\rho_m) + \nabla \cdot (\rho_m \bar{v}_m) = 0 \quad (1)$$

\bar{v}_m indicates the average speed of mass:

$$\bar{v}_m = \frac{\sum_{k=1}^n \alpha_k \rho_k \bar{v}_k}{\rho_m} \quad (2)$$

ρ_m indicates mixture density:

$$\rho_m = \sum_{k=1}^n \alpha_k \rho_k \quad (3)$$

α_k indicates the volume fraction of K phase.

(2) Momentum equation:

The momentum equation of the mixed phase can be accumulated by the momentum equation of all phases. The formula is as follows:

$$\begin{aligned} \frac{\partial}{\partial t}(\rho_m \bar{v}_m) + \nabla \cdot (\rho_m \bar{v}_m \bar{v}_m) = -\nabla p \\ + \nabla \cdot \left[\mu_m (\nabla \bar{v}_m + \nabla \bar{v}_m^T) \right] + \rho_m \bar{g} + \bar{F} + \nabla \cdot \left(\sum_{k=1}^n \alpha_k \rho_k \bar{v}_{dr,k} \bar{v}_{dr,k} \right) \end{aligned} \quad (4)$$

n indicates the number of phases; \bar{F} indicates the volume force and μ_m indicates the viscosity of the mixed phase:

$$\mu_m = \sum_{k=1}^n \alpha_k \rho_k \quad (5)$$

$\bar{v}_{dr,k}$ indicates the drift velocity of sub phase K:

$$\bar{v}_{dr,k} = \bar{v}_k - \bar{v}_m \quad (6)$$

(3) relative (slip) velocity and drift velocity:

The relative velocity (also known as slip velocity) is defined as the speed of the sub phase p relative to the main phase q:

$$\bar{v}_{pq} = \bar{v}_p - \bar{v}_q \quad (7)$$

The mass fraction of k in any phase can be defined as:

$$c_k = \frac{\alpha_k \rho_k}{\rho_m} \quad (8)$$

The drift velocity and relative velocity are established through the following formula:

$$\vec{v}_{dr,p} = \vec{v}_{pq} - \sum_{k=1}^n c_k \vec{v}_{qk} \quad (9)$$

The algebraic slip formula is used in a mixture model in Fluent. The basic assumption of the algebraic slip model is that in order to clarify the algebraic relationship of the relative velocity, the local equilibrium phase should be achieved in a short time period. According to Manninen, the relative form is

$$\vec{v}_{pq} = \frac{\tau_p}{f_{drag}} \frac{(\rho_p - \rho_m)}{\rho_p} \vec{a} \quad (10)$$

τ_p indicates the relaxation time of particles.

$$\tau_p = \frac{\rho_p d_p^2}{18 \mu_q} \quad (11)$$

d in the formula represents the diameter of p particles (droplets or bubbles), and \vec{a} indicates the acceleration of the sub phase particles:

$$f_{drag} = \begin{cases} 1 + 0.15 \text{Re}^{0.687} & (\text{Re} \leq 1000) \\ 0.0183 \text{Re} & (\text{Re} > 1000) \end{cases} \quad (12)$$

The acceleration \vec{a} is determined by the following:

$$\vec{a} = \vec{g} - (\vec{v}_m \cdot \nabla) \vec{v}_m - \frac{\partial \vec{v}_m}{\partial t} \quad (13)$$

(4) The sub phase volume fraction equation:

The volume fraction equation can be obtained from the continuity equation of the sub phase P:

$$\frac{\partial}{\partial t} (\alpha_p \rho_p) + \nabla \cdot (\alpha_p \rho_p \vec{v}_m) = -\nabla \cdot (\alpha_p \rho_p \vec{v}_{dr,p}) + \sum_{q=1}^n (\dot{m}_{qp} - \dot{m}_{pq}) \quad (14)$$

The self-priming process of the self-priming pump is studied on the basis of solving the time problem, and its solution method is a transient solution [Li, Xu, Li et al. (2013); Li, Wu, Wang et al. (2010); Wang, Tan and Wang (2013); Li, Wu, Dai et al. (2010)]. In order to more accurately conform to the actual situation, the gravity of the fluid is considered. The physical models are the standard k-ε turbulence model and the mixture multiphase flow model, and the wall function is the standard wall function [Fu, Yuan, Zhu et al. (2012)]. The simulation involves two-phase conditions, so it is necessary to set two phases separately, selecting water as the main phase and air as the secondary phase. Rotational coordinates are used to define the rotational motion of the rotor components, whose rotational speed is of n=2900 r/min, rotating right along the Z axis. The inlet boundary condition is set as the velocity inlet, and the direction is the normal direction of the inlet surface. In order to make the simulation process more consistent

with the actual situation, tests of other self-priming pumps can be referred to. The import speed is a piecewise function, which is related to the time. When $0 < t \leq 100$, the speed is 0.24. When $100 < t \leq 120$, the speed is $0.05809t - 5.569$. When $t > 120$, the speed is 1.4018. The inlet speed is programmed with the UDF function of Fluent. The code is as follows:

```
#include "udf.h"
DEFINE_PROFILE(velocity,thread,position)
{
    real t=CURRENT_TIME;
    face_t f;
    begin_f_loop(f,thread)
    {
        if(t>0&&t<=100)
            F_PROFILE(f,thread,position)=0.24;
        else if(t>100&&t<=120)
            F_PROFILE(f,thread,position)=0.05809*t-5.569;
        else
            F_PROFILE(f,thread,position)=1.4018;
    }
    end_f_loop(f,thread)
}
```

Except that the rotor is defined as rotating wall, the outlet boundary is set as free outflow, and other boundary conditions are set as fixed wall. According to the rotational speed and number of blades of the self-priming pump, in order to capture the instantaneous characteristics of the self-priming process, the calculation time step is as follows:

$$\Delta t = \frac{60}{4n} = \frac{60}{4 \times 2900} = 0.00517 \text{ (s)} \quad (15)$$

The velocity-pressure coupled PISO algorithm is used to solve the problem. For the space discretization, the pressure standard discretization, momentum, volume fraction, turbulent kinetic energy and turbulent dissipation rate, the first-order upwind difference scheme is used to reduce the difficulty of convergence. The global initialization method is used to initialize the results. The liquid phase and the gas phase are separated in the initial state. The water-filled part below the outlet of the volute is defined as the liquid part. The other parts of the computational domain are all filled with air in the initial state. The distribution of gas-liquid two-phase flow in the self-priming pump after initialization in Fluent is shown in Fig. 3. The red part shows liquid water, and the blue part shows gas phase air.

In order to shorten the calculation time, the time step is changed by 0.00517 s, 0.01 s, 0.1 s and 1 s. The maximum number of iteration steps is set to 100 steps and the total calculation time is 160 s. The whole self-priming process is divided into three stages: the initial stage of self-priming (0-30 s), which mainly cleans the air in the inlet section to let the water enter the inhalation section smoothly; the stable self-priming process (30-140 s), as a stable self-priming process, which is less than 0.1 from the beginning of the inhalation section to the air content in the self-priming pump; the final stage of self-priming (140-160 s). This process is mainly to discharge the remaining small amount

of air in the self-priming pump.

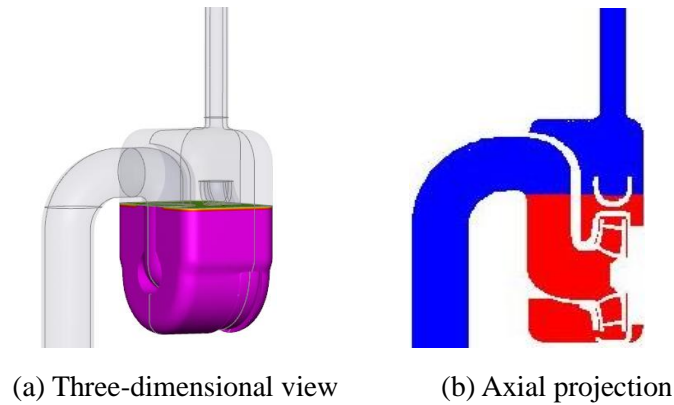


Figure 3: Air-water distribution in the initial state of the self-priming pump

2.3 Models of different reflux hole schemes

The area and location of the reflux hole will affect the self-priming performance of the self-priming pump. To investigate the influence of reflux hole area on the self-priming process, the area of the reflux hole was adjusted while the position of the reflux hole remained unchanged. The model of reflux holes for different schemes is shown in Fig. 4. The area of the reflux hole of the four different schemes is shown in Tab. 2.

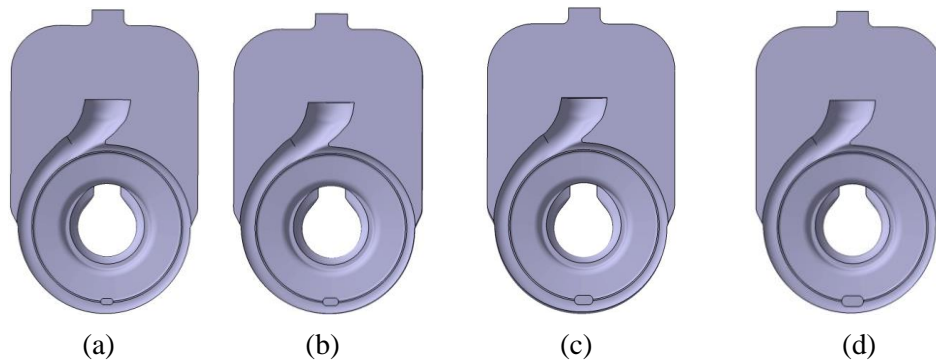


Figure 4: Different reflux hole areas

Table 2: Reflux hole area for different schemes

	a	b	c	d
Reflux hole area AH/(mm ²)	141.26	178.54	257.1	349.94

3 Self-priming process analysis

3.1 Analysis of monitoring surface parameters

The self-priming process of the self-priming pump was numerically calculated with different reflux hole areas. The inlet, outlet and reflux hole sections of the self-priming pump were selected as monitoring surfaces. The flow rate and air volume fraction of the reflux hole over the entire self-priming process were analyzed.

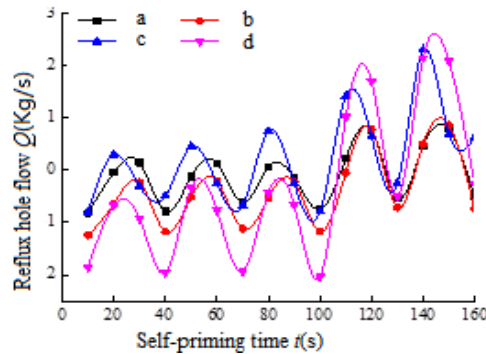


Figure 5: Flow rate of reflux holes

Fig. 5 shows the flow rate of the reflux holes with different areas. The positive and negative flow rate indicate the flow direction of the fluid; the flow direction from the pump cavity into the impeller is positive, and the reverse is negative. It can be seen that the change trend of the flow rate of the reflux hole is the same for the different schemes. Not only does the flow rate change, but also the flow direction changes. In scheme c, peak traffic volume precedes other schemes, and peak traffic volume before 100 s is larger than in other schemes.

Fig. 6 shows the air volume fraction of the reflux hole under the different schemes. It can be seen that before 140 s, the air volume fraction of scheme c is obviously larger than that of the other three schemes, and the air-water mixture flowing through the reflux hole has a larger air integral and is fully mixed with water. After 140 s, the air volume fraction of the reflux hole of the four schemes basically decreased to 0.

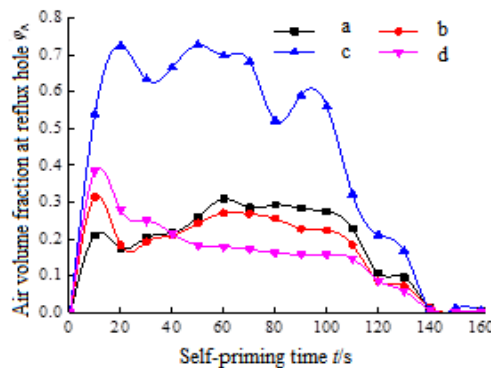


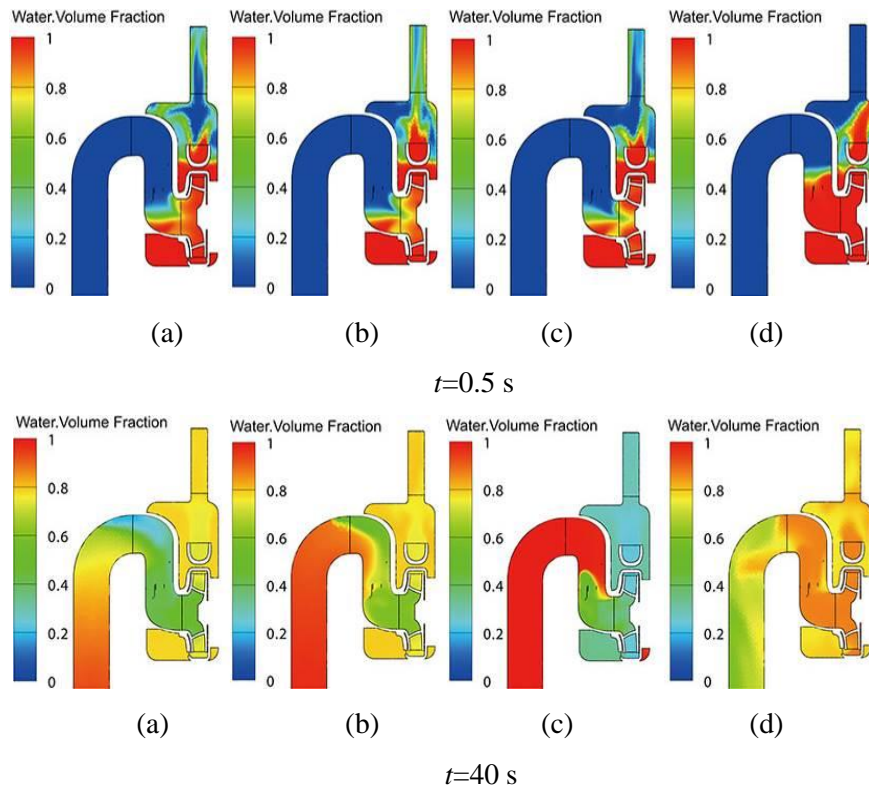
Figure 6: Air volume fraction of reflux hole

3.2 Axial distribution of gas and water during the self-priming process

In the self-priming process, in order to more intuitively and clearly reflect the distribution of gas and water, $Y=0$ axial surface was selected to monitor the distribution of gas and water in the self-priming pump at different times to study the flow characteristics over the entire process.

As shown in Fig. 7, when $t = 0.5$ s, water is sucked into the impeller and flows through the volute to mix with air in the gas-liquid separation chamber. Part of the water enters the discharge pipe section and gradually discharges with the process of self-priming. The distribution of gas and water on the axial surface of scheme a, b and c is not very different. Most of the water in the suction section has entered the impeller, while only a small part of the water in scheme d enters the impeller, and more water is discharged from the outlet of the volute.

In the process of self-priming, when $t=40$ s, a part of the water in the intake pipe of scheme a has entered the suction section. The air in the intake section of scheme b has basically been discharged. The water has filled the entire intake pipe, and a large amount of water has flowed into the suction section. In scheme c, about half of the space in the suction section is fully filled with water. In scheme d, there is still a large amount of air in the intake pipe. The suction section and the impeller are a mixture of air and water. The water content in the suction section is relatively small while the distribution is relatively uniform in the space.



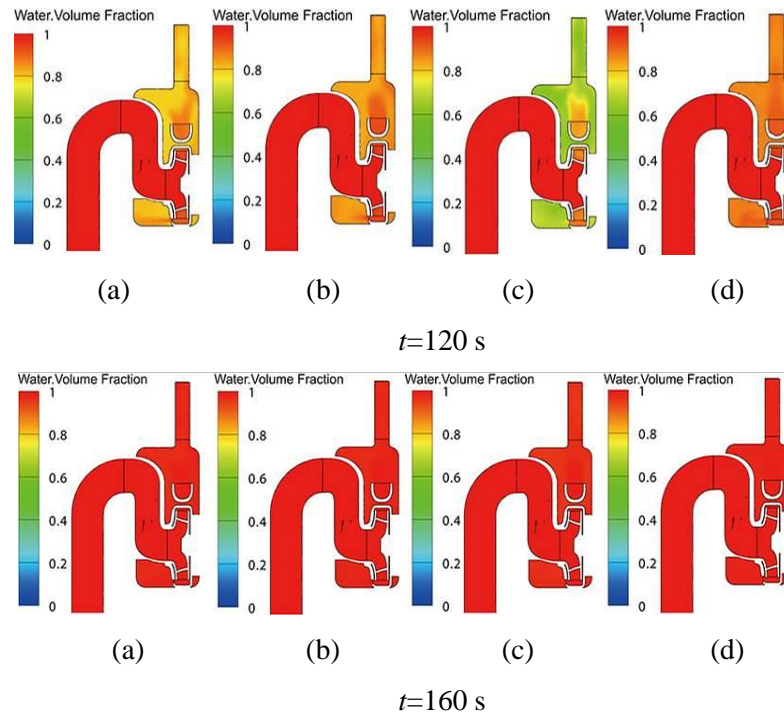


Figure 7: Air-water distribution of the different schemes in the self-priming process

When $t=120\text{ s}$, the air in the intake pipe, suction section and impeller of the four schemes has basically been exhausted, all filled with water. There is a small amount of residual air in the volute, and the air volume fraction in the pump chamber and the outlet pipe is higher than that in other places. The air in the pump chamber of scheme d is less than the other three schemes and the distribution of air and water is relatively uniform. This shows that the larger the reflux hole is, the more conducive to the mixing of air and water, and the more easily the air is discharged from the self-priming pump. The air volume fraction in the outlet pipe of scheme d is obviously lower than that of the other schemes.

When $t=160\text{ s}$, the air volume fraction of the four schemes is basically 0. The residual air in the self-priming pump is basically exhausted, and the whole self-priming process is basically completed. After that, the self-priming pump will enter the normal operation stage; the fluid medium in the self-priming pump is no longer a gas-water mixture, but pure water. In the whole self-priming process, with the increase of reflux hole area, the mixture of air and water becomes more and more full and uniform; the distribution of gas and water becomes more and more uniform, and the self-priming time of the self-priming pump reduces gradually. In the self-priming process, scheme c is the quickest to suck water from the intake pipe into the impeller. Although the self-priming time decreases with the increase of the area of the reflux hole, when the area of the reflux hole is too large, the return flow through the reflux hole is also large, which reduces the efficiency of the self-priming pump. Considering the self-priming time and its performance, the reflux hole of scheme c is the best of the four schemes.

3.3 Isosurface distribution of air volume fraction at the end of self-priming

In order to capture the moment more accurately when the self-priming pump completes the self-priming process, the air volume fraction isosurface map is used to monitor the value of air volume fraction at the end of self-priming. When the air volume fraction is equal to or very close to zero, the self-priming pump basically completes the self-priming process, and the self-priming pump enters the normal operation state. Four time points of self-priming, $t=120$ s, $t=130$ s, $t=140$ s and $t=160$ s, were selected to monitor the change of air volume fraction isosurface in the self-priming pump, so as to capture the process of air volume fraction reduction and the end of the self-priming process.

When $t=120$ s, with the increase of reflux hole area, the isosurface maps of air volume fraction in the self-priming pump are 0.21, 0.17, 0.30 and 0.13 respectively. In scheme a, the isosurface of the air volume fraction is mainly located near the outlet of the pump chamber at the upper right side of the pump chamber. In scheme b, the air volume fraction isosurface is mainly at the outer edge of the pump chamber and near the outlet of the air-liquid separation chamber. The volume fraction of air in scheme c is less than 0.3, and the isosurface is mainly located at the left outer edge of the pump cavity and the bottom of the pump cavity near the reflux hole. In scheme d, the isosurface of air volume fraction is located at the outer edge of the pump chamber and part of the outer edge of the volute.

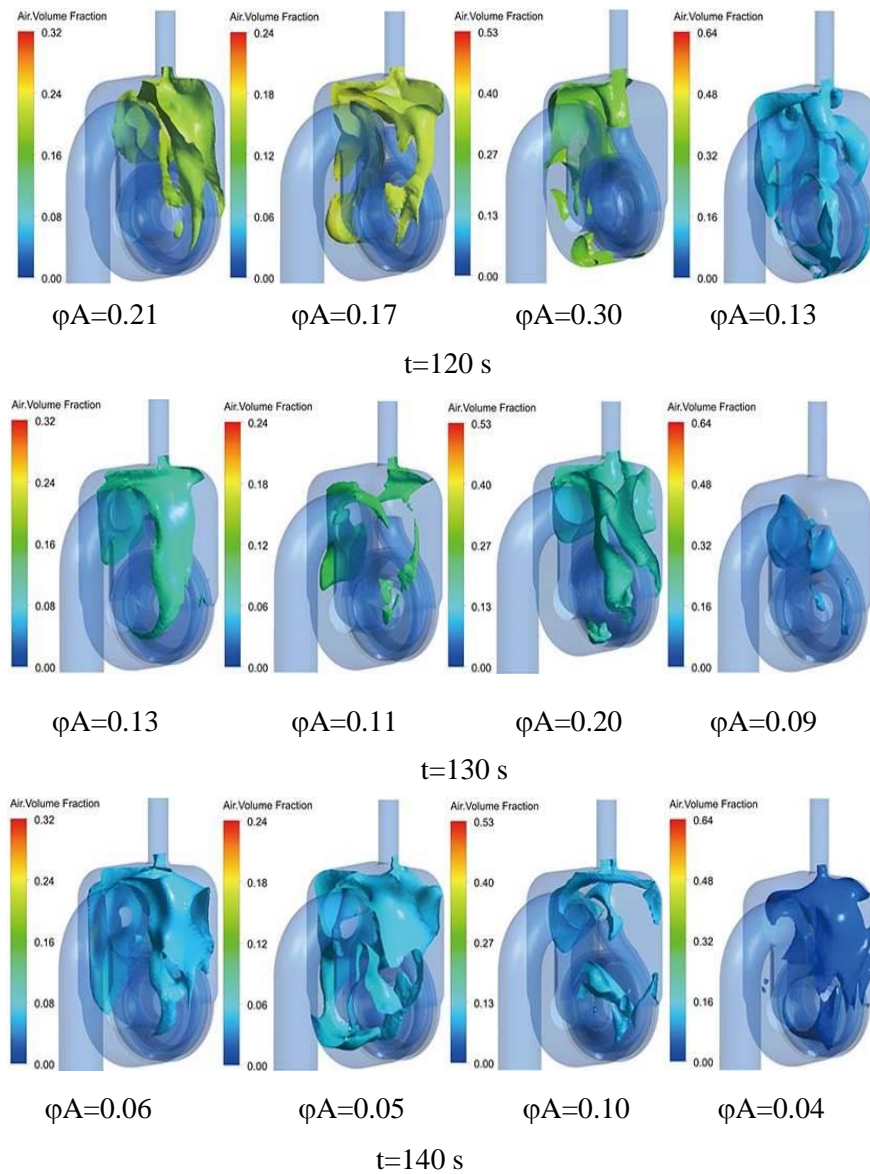
When $t=130$ s, the air volume fraction of the four schemes is below 0.13, 0.11, 0.20 and 0.09 respectively. In the first scheme, the isosurface of the air volume fraction is on the right outer edge of the pump chamber and near the outer side of the outlet side. In scheme b, the range of the isosurface is small, and the distribution area is the local area near the suction section and the exit on the right side of the pump cavity. The isosurface in scheme c is a small area near the recirculation hole and a part of the outer edge of the pump chamber. In scheme d, the air volume fraction isosurface is distributed in the middle of the pump chamber near the suction side and the outer edge of the volute.

When $t=140$ s, the air volume fraction is reduced to less than 0.1. The values of the air volume fraction isosurface of scheme a and scheme b are 0.06 and 0.05 respectively. This indicates that the air volume fraction in the self-priming pump is already small, and the distribution range of the isosurface of the two schemes is large. It is distributed mostly in areas of the outer edge of the pump chamber, and there is no distribution at the bottom of the pump chamber. In the third scheme, the isosurface is distributed only in small areas, concentrating on the outlet of the pump chamber and the middle and lower parts. The isosurface in the fourth scheme is mainly distributed in some parts of the outer edge of the pump chamber.

When $t=160$ s, the air volume fraction of scheme a and b is below 0.01, and for scheme c and d it is below 0.005. At this time, it can be considered that the self-priming pump has completed the self-priming process; the air in the self-priming pump has basically been exhausted. In scheme c, the distribution range of air volume fraction isosurface is the smallest, indicating that the area of air volume fraction below 0.005 is smaller, and the residual air in the self-priming pump is less.

It can be seen from Fig. 8 that the value of the air volume fraction isosurface decreases gradually with the increase of the area of the reflux hole in schemes a, b and d. This

indicates that the less the residual air in the self-priming pump, the closer the self-priming pump is to completion. With the increase of the area of the reflux hole, the air in the self-priming pump is more easily discharged and the self-priming time is shorter. In scheme c, the value of the air volume fraction isosurface at 120 s-140 s is higher than in the other three schemes, while the distribution area is small, which indicates that the residual air in the self-priming pump distribution range is small. At 160 s, the air volume fraction value has dropped to the same as of scheme d. Considering the self-priming time should be shortened as far as possible in the process of self-priming, and the air distribution in the self-priming pump should not be too wide, the area of reflux hole in scheme c is the most suitable.



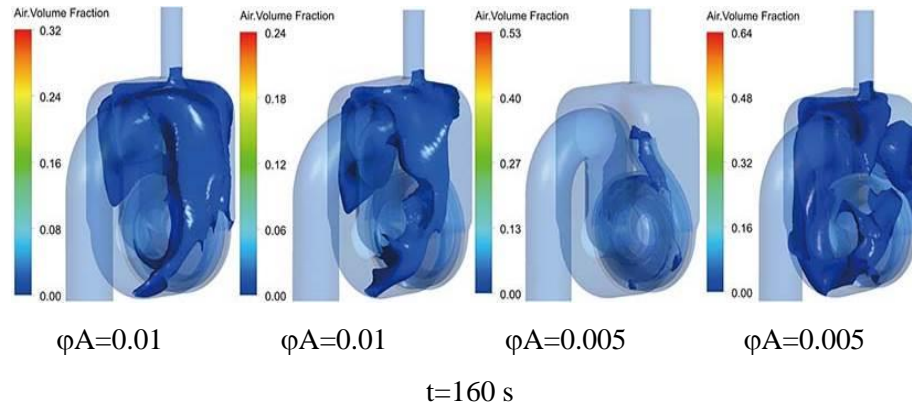


Figure 8: Isosurface of air volume fraction at the end of the self-priming process with different reflux holes

3.4 Cross section streamline distribution in the process of self-priming

A streamline diagram can reflect the flow characteristics in the self-priming pump at different times, and it is more convenient to observe the flow field distribution and speed. The streamline distribution of $Z=0$ cross section at $t=0.5$ s, $t=10$ s, $t=40$ s and $t=160$ s is selected to analyze the streamline distribution at different time points in the entire self-priming process, and the variation of flow is obtained.

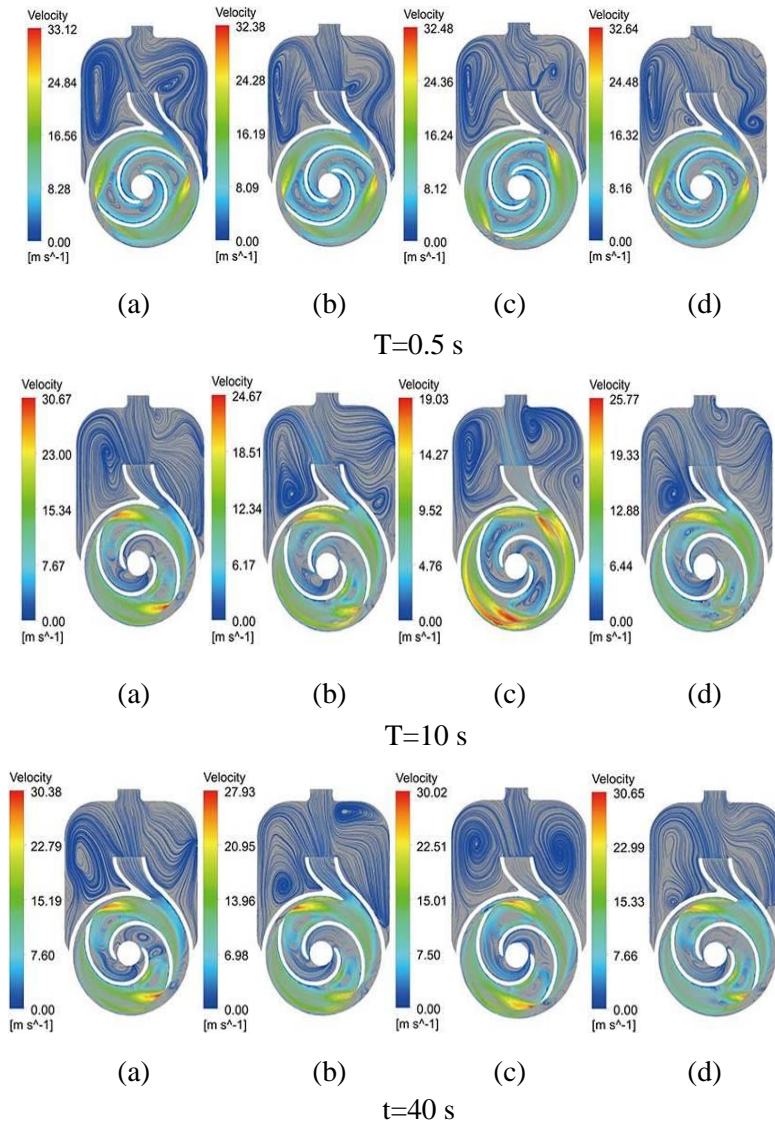
When $t = 0.5$ s, the maximum velocities of the four schemes appear at the trailing edge of the impeller outlet blade, which are 33.12 m/s, 32.38 m/s, 32.48 m/s and 32.64 m/s respectively. In scheme a, there is a narrow elliptical vortex on the left side of the pump chamber and an elliptical vortex near the volute outlet on the right side of the pump chamber. In scheme b, the elliptical vortex on the left side of the pump chamber is closer to the outer edge of the pump chamber, and the vortex on the right side is smaller than in scheme a. In scheme c, there is an elliptical vortex on the left side of the pump chamber, and a circular and elliptical vortex on the right side. In scheme d, the elliptical vortex appears on the left side of the pump cavity, and the vortex on the right side of the pump cavity is close to the lower side.

When $t=10$ s, the maximum velocity in scheme a is 30.67 m/s. The vortex on the left side of the pump cavity becomes circular, and the vortex on the right side disappears. In scheme b, the maximum velocity is 24.67 m/s, and there is a vortex on the left and right sides of the pump cavity near the volute. In scheme c, the maximum velocity is 19.03 m/s at the trailing edge of the blade and the outer edge of the volute at the outlet of the impeller. There is a vortex near the outer edge of the pump chamber and the outlet at the left and right sides of the gas-liquid separation chamber. In scheme d, the maximum velocity is 25.77 m/s, and a small vortex is formed near the outer edge of the volute on the left side of the pump chamber.

When $t=40$ s, the maximum velocity at the trailing edge of the impeller outlet blade is 30.38m/s, 27.93 m/s, 30.02 m/s and 30.65 m/s respectively. The location of the vortex in scheme a is the left outer edge of the pump chamber. The scheme b vortex appears in the pump cavity near the outer edge and the upper edge of the volute pump cavity. The two

vortices in scheme c basically distribute symmetrically on the left and right sides of the pump cavity. In scheme d, a smaller vortex is formed on the left side of the pump chamber and the outer edge of the volute.

When $t=160$ s, the self-priming process of the self-priming pump is basically over. The maximum speed of the four schemes is 25.01 m/s, 26.39 m/s, 25.28 m/s and 34 m/s respectively. The vortices in scheme a, b and d are formed at the upper left side of the pump cavity. The range of vortices in scheme b is wider than that in scheme a. There is a vortex formed on the left and right sides of the pump chamber.



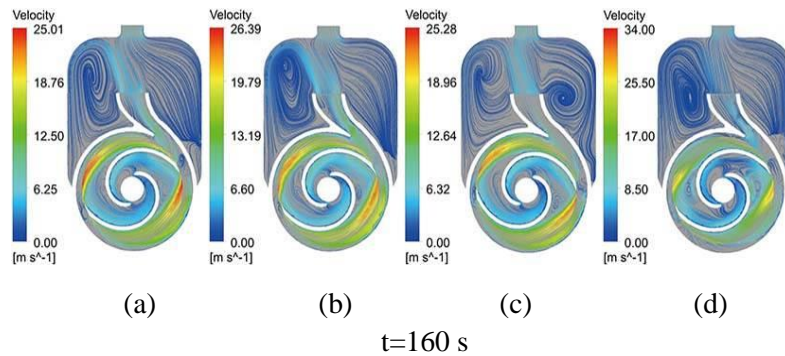


Figure 9: Cross section streamline diagram of the process of self-priming

In conclusion, the maximum velocity appears at the trailing edge of the impeller outlet blade during the self-priming process. With the development of the self-priming process, the regions with greater velocity are slightly different. Vortices appear in the pump cavity, and the number and position of vortices is different in the self-priming process at different times. In the process of self-priming, although the pump chamber has large space and small flow velocity, the flow situation is complex, with a gas-liquid mixture and separation, accompanied by the formation of vortices and the development of movement.

4 Analysis of experimental data

A closed test console, with high precision and wide application in enterprises, is used to control the test and collect the corresponding parameters. The fluid medium used in this experiment is clean water at room temperature. After normal water delivery, the pressure, flow rate, axial force and rotational speed of the inlet and outlet of the pump are measured. By adjusting the flow rate of the pump, the head, power and efficiency data of the pump under different flow conditions are obtained.

The external characteristic curve of the self-priming pump and the efficiency of the self-priming pump with different reflux hole areas are obtained by experiments, and the results are compared with the simulation results. In order to verify the correctness of the numerical calculation by comparing the simulation results with the experimental data, and to verify each in the numerical calculation domain, the $Q-H$ and $Q-\eta$ diagrams obtained from the experiment and numerical calculation under the optimal reflux hole area ($A_H = 257.1 \text{ mm}^2$) are plotted in the same coordinate system, as shown in Fig. 10.

It can be seen from Fig. 10 that the pump head decreases gradually with the increase of flow rate, and the pump efficiency increases first and then decreases. At rated flow, the maximum pump efficiency is 65%. At this time, the pump head is 40 m. The change of pump head and efficiency with the flow rate conforms to the variation law of the corresponding parameters when the pump is running.

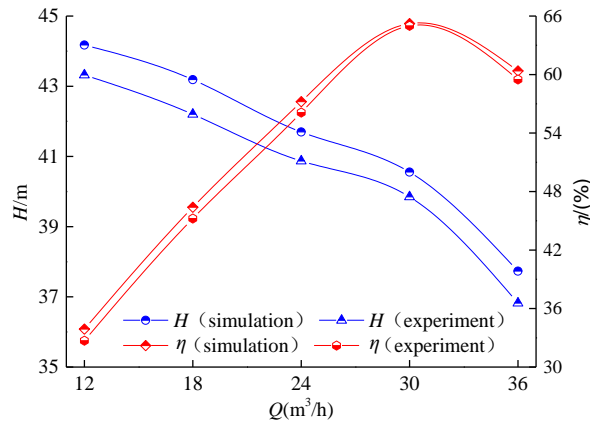


Figure 10: Q - H and Q - η curves of self-priming pump ($A_H=257.1 \text{ mm}^2$)

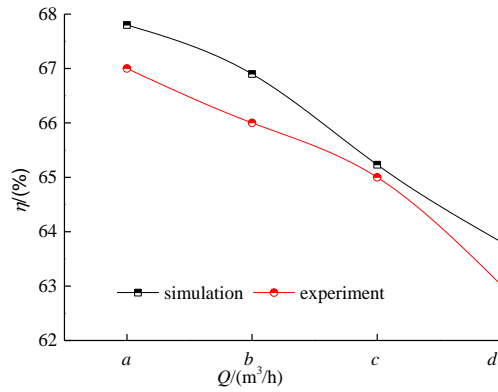


Figure 11: Design flow rate of Q - η curve with different reflux hole areas

Under the designed flow rate, the efficiency of the self-priming pump with different reflux hole areas are distinguished, and the Q - η curves of the self-priming pump with different schemes are obtained. As shown in Fig. 11, the efficiency of the self-priming pump decreases gradually with the increase of the area of the reflux hole. Especially when the area of the reflux hole increases from scheme c to scheme d, the efficiency and performance of the self-priming pump decreases rapidly. The match between the simulated value of scheme c and the data obtained from the experiment is relatively high. Under the other three schemes, the difference between the simulated values and the experimental values is relatively large, but still within the allowable range of error.

5 Conclusions

1) Under the four different schemes, the variation trend of the reflux hole flow is basically the same. In scheme c, the peak value of flow is reached sooner than in the other schemes, and the volume fraction of gas at the reflux hole is higher than in the other three schemes. The gas-water mixture is sufficient, as is the flow into the gas-liquid

separation chamber for separation, so the air can be expelled from the pump chamber as soon as possible.

2) The larger the area of the reflux hole is, the shorter the self-priming time is. However, when the area is too large, the return flow through the reflux hole is also large, which reduces the efficiency of the self-priming pump. Through the analysis and comparison of the axial gas-water distribution and the air volume fraction distribution at the end of the self-priming process under different schemes, it is found that the area of the reflux hole in scheme c is most appropriate.

3) According to the streamline distribution of the cross section at different times, it can be seen that the maximum velocity is at the blade trailing edge of the impeller outlet, and the maximum velocity occurs at different times. The flow in the pump chamber is complex and accompanied by the formation of vortices. The number, shape and position of vortices change.

4) Comparing the experimental data with the calculated results, and considering the influence of reflux hole area on the self-priming time and efficiency, the optimum area is in scheme c.

5) The experimental study only studied the influence of reflux hole area on the external characteristics of the self-priming pump. The influence of other geometric parameters of the self-priming pump on its external characteristics and self-priming performance has not been studied.

References

Fang, C. F. (2018): Study on the application of self suction pump in makeup water intake engineering of power plant. *Construction & Design for Engineering*, vol. 12, pp. 68-70.

Fu, Q.; Yuan, S. Q.; Zhu, R. S.; Wang, X. L. (2012): Hydraulic characteristics of transient transition process of gas-liquid mixed flow in a centrifugal pump. *Journal of Harbin Engineering University*, vol. 33, no. 11, pp. 1428-1434.

Guan, X. F. (2011): *Theory and Design of Modern Pump*. Beijing: China Aerospace Publishing House.

Huang, S.; Su, X. H.; Guo, J. (2014): Unsteady numerical simulation for gas-liquid two-phase flow in self-priming process of centrifugal pump. *Energy Conversion and Management*, vol. 85, no. 9, pp. 694-700.

Jiang, H.; Xie, Y. H.; Wang, C.; Zhao, F. (2014): Research on the status of self-priming centrifugal pump. *Energy Conservation*, vol. 11, pp. 70-74.

Kanute, J. (2004): Self-priming centrifugal pumps: a primer. *World Pumps*, vol. 456, pp. 30-32.

Li, H.; Chen, C.; Yuan, S. Q.; Gao, Z. J. (2015): Current situation and suggestions for its development of small-scale sprinkler irrigation machine in China. *Journal of Drainage and Irrigation Machinery Engineering*, vol. 33, no. 4, pp. 356-361.

Li, H.; Jiang, B.; Lu, T. Q. (2015): Visualization experiment of gas-liquid two-phase flow of pump during self-priming process. *Transactions of the Chinese Society for Agricultural Machinery*, vol. 46, no. 8, pp. 59-65.

Li, H.; Xu, D. H.; Li, L.; Tu, Q.; Zhou, C. H. (2013): Numerical simulation of transient flow in self-priming centrifugal pump during self-priming period. *Journal of Drainage*

and Irrigation Machinery Engineering, vol. 31, no. 7, pp. 565-569.

Li, Z. F.; Wu, D. Z.; Dai, W. P.; Chen, F. Q. (2010): Experimental study on transient characteristics and flow of centrifugal pump during startup. *Journal of Engineering Thermophysics*, vol. 31, no. 12, pp. 2019-2022.

Lin, R.; Yan, C. Q.; Xia, M. Z. (2014): Hydraulic design and self-priming performance test of self-priming pump. *Technology Innovation and Application*, vol. 36, pp. 41-42.

Li, Z. F.; Wu, D. Z.; Wang, L. Q.; Dai, W. P.; Chen, F. Q. (2010): Experiment on instantaneous characteristics in centrifugal pump during startup period. *Journal of Drainage and Irrigation Machinery Engineering*, vol. 28, no. 5, pp. 389-393.

Liu, H. S.; Su, Y. S. (2017): Numerical simulation of gas-liquid two-phase flow in self-priming pump during self-priming period. *Journal of East China University of Science and Technology (Natural Science Edition)*, vol. 43, no. 2, pp. 280-285.

Liu, J. R.; Su, Q. Q. (2009): Numerical simulation oil gas-liquid two-phase flow in self-priming pump. *Transactions of the Chinese Society for Agricultural Machinery*, vol. 40, no. 9, pp. 73-76.

Ma, X. J.; Zhang, Y. Q.; Cui, S. L.; Zhang, C.; Lin, S. J. (2018): Study on reflux hole size's influence on the self-priming pump performance. *Journal of Gansu Sciences*, vol. 30, no. 2, pp. 98-102.

Mou, J.; Wang, H.; Wu, D. H.; Ren, Y.; Shi, Z. Z. et al. (2018): Flows and distribution patterns of solid particles in sewage self-priming pump. *Journal of Hydroelectric Engineering*, vol. 37, no. 7, pp. 48-57.

Pan, Z. Y.; Zhang, D. Q.; Li, Y. J.; Pan, X. W. (2014): Design and analyses of sprinkler irrigation and drip irrigation dual-use self-priming pump. *Journal of Huazhong University of Science and Technology (Natural Science Edition)*, vol. 3, pp. 122-126.

Lu, T. Q.; Li, H.; Zhan, L. C. (2016): Transient numerical simulation and visualization of self-priming process in self-priming centrifugal pump. *Journal of Drainage & Irrigation Machinery Engineering*, vol. 34, no. 11, pp. 927-933.

Wang, C.; Shi, W. D.; Li, W.; Zhang, D. S.; Jiang, X. P. (2016): Unsteady numerical calculation and validation on self-priming process of self-priming spray irrigation pump. *Transactions of the Chinese Society of Agricultural Engineering*, vol. 32, no. 16, pp. 65-72.

Wang, C. L.; Wu, Z. W.; Si, Y. L.; Yi, T. X.; Liu, H. G. (2009): Gas-liquid two-phase flow numerical simulation of a vortex flow self-priming pump. *Drainage and Irrigation Machinery*, vol. 27, no. 3, pp. 163-167.

Wang, S. L.; Tan, L.; Wang, Y. H. (2013): Characteristics of transient cavitation flow and pressure fluctuation for a centrifugal pump. *Journal of Vibration and Shock*, vol. 32, no. 22, pp. 168-173.

Wang, Y. Y. (2014): The influence factors of self-priming pump self-priming performance. *Hunan Agricultural Machinery*, vol. 41, no. 7, pp. 95-96.

Xiao, L.; Long, X. (2015): Cavitating flow in annular jet pumps. *International Journal of Multiphase Flow*, vol. 71, no. 5, pp. 116-132.

Yuan, S. Q.; Li, H.; Shi, W. D. (2011): *Design Theory and Technology of New Spray*

Irrigation Equipment. Beijing: China Machine Press.

Yuan, S. Q.; Li, H.; Wang, X. H. (2015): Status, problems, trends and suggestions for water-saving irrigation equipment in China. *Journal of Drainage and Irrigation Machinery Engineering*, vol. 33, no. 1, pp. 78-92.

Yuan, S. Q. (2015): *Technology and Equipment of Spray Micro Irrigation*. Beijing: China Water Power Press.

Zhou, J. M.; Zhang, L. Q.; Sichuan Petrochemical Company (2018): Successful application of a simple self-priming pump in circulating water field. *Petrochemical Industry Technology*, vol. 6, pp. 60, 67.